



## OPEN

## SUBJECT AREAS:

SYNTHESIS OF  
GRAPHENE

CHEMICAL ENGINEERING

SOLAR CELLS

SYNTHESIS OF GRAPHENE

# In-situ electrochemically deposited polypyrrole nanoparticles incorporated reduced graphene oxide as an efficient counter electrode for platinum-free dye-sensitized solar cells

Received  
15 April 2014Accepted  
27 May 2014Published  
16 June 2014Su Pei Lim<sup>1</sup>, Alagarsamy Pandikumar<sup>1</sup>, Yee Seng Lim<sup>1</sup>, Nay Ming Huang<sup>1</sup> & Hong Ngee Lim<sup>2,3</sup>

<sup>1</sup>Low Dimensional Materials Research Centre, Department of Physics, Faculty of Science, University of Malaya, 50603 Kuala Lumpur, Malaysia, <sup>2</sup>Department of Chemistry, Faculty of Science, Universiti Putra Malaysia, 43400 UPM Serdang, Selangor, Malaysia, <sup>3</sup>Functional Device Laboratory, Institute of Advanced Technology, Universiti Putra Malaysia, 43400 UPM Serdang, Selangor, Malaysia.

Correspondence and requests for materials should be addressed to

A.P.

(pandikumarinbox@gmail.com); N.M.H. (huangnayming@um.edu.my) or H.N.L. (janet\_limhn@yahoo.com)

This paper reports a rapid and in-situ electrochemical polymerization method for the fabrication of polypyrrole nanoparticles incorporated reduced graphene oxide (rGO@PPy) nanocomposites on a ITO conducting glass and its application as a counter electrode for platinum-free dye-sensitized solar cell (DSSC). The scanning electron microscopic images show the uniform distribution of PPy nanoparticles with diameter ranges between 20 and 30 nm on the rGO sheets. The electrochemical studies reveal that the rGO@PPy has smaller charge transfer resistance and similar electrocatalytic activity as that of the standard Pt counter electrode for the  $I_3^-/I^-$  redox reaction. The overall solar to electrical energy conversion efficiency of the DSSC with the rGO@PPy counter electrode is 2.21%, which is merely equal to the efficiency of DSSC with sputtered Pt counter electrode (2.19%). The excellent photovoltaic performance, rapid and simple fabrication method and low-cost of the rGO@PPy can be potentially exploited as a alternative counter electrode to the expensive Pt in DSSCs.

In view of the concerns relevant to natural resource depletion and environmental pollution problems and to eradicate the same, dye-sensitized solar cell (DSSC) has appeared to be a promising potential candidate for the production of electricity from solar energy in an efficient and eco-friendly manner<sup>1</sup>. Recently, several efforts have been made to enhance the performance of DSSC, such as introduction of novel photoanodes, electrolytes, dyes and counter electrodes<sup>1</sup>. Among them, counter electrode plays a crucial role in increasing the conversion efficiency of the DSSC as it serves as a mediator for collecting electrons from the external circuit, reduces  $I_3^-$  into  $I^-$  and moreover it regenerates the oxidized dye after electron injection<sup>1</sup>. The efficient counter electrodes can reduce internal energy loss in DSSCs and thus produce higher current densities and fill factors<sup>1</sup>. So far, the most preferred material for counter electrode in DSSC is platinum (Pt), due to its excellent electrocatalytic activity towards  $I_3^-$  reduction<sup>1</sup>. However, the high-cost and the rarity of Pt significantly hinder its practical application in DSSCs, including mass production and commercialization<sup>1</sup>. This has promoted large research interest in exploring alternative counter electrode materials for Pt-free DSSCs. In the past decades, carbon-based materials<sup>2-8</sup>, conducting polymers<sup>6,9</sup> and transition metal based inorganic materials<sup>10-12</sup> have been used as counter electrode materials and they showed reliable conversion efficiencies in DSSCs like Pt-based counter electrode.

Recently, carbonaceous materials, such as graphite, activated carbon, single-walled carbon nanotubes (SWCNTs), double-walled carbon nanotubes (DWCNTs), multi-walled carbon nanotubes (MWCNTs) and graphene have been employed as potential alternative counter electrode materials, due to their high electronic conductivity, corrosion resistance towards  $I_2$ , high reactivity for  $I^-$  reduction and low-cost<sup>1,13-15</sup>. Among them, graphene<sup>16</sup>, which is an atomic planar sheet of hexagonally arrayed  $sp^2$  carbon atoms has been demonstrated to be a promising and efficient counter electrode material for DSSCs, because of its excellent conductivity and high electrocatalytic activity<sup>1,17</sup>. Even though, some reports revealed that the bare graphene alone does not to be the



right candidate for a counter electrode in DSSCs, owing to the limited number of active sites for the  $I_3^-/I^-$  electrocatalytic reaction<sup>8</sup>. For this reason, further efforts have been undertaken based on the conducting polymers, such as poly(3,4-ethylenedioxythiophene)-poly(styrenesulphonate) (PEDOT:PSS), polypyrrole (PPy) and polyaniline (PANI) incorporated into graphene for DSSC applications because of their merits of both excellent electron conductivity and high catalytic activities<sup>18–20</sup>. Among the conducting polymers, polypyrrole (PPy) is an excellent and suitable counter electrode material because of its desirable features, including low-cost, environmental stability and large scale processability<sup>21</sup>.

In this work, we report a simple and rapid fabrication method for the preparation of polypyrrole-reduced graphene oxide (rGO@PPy) nanocomposite materials and their application as counter electrode for Pt-free DSSCs. The formation of PPy nanoparticles incorporated reduced graphene oxide nanocomposite film is achieved by a rapid and in-situ electrochemical polymerization method. Previously, Gong *et.al.* reported the chemical polymerization method for the fabrication of PPy incorporated with graphene for counter electrode in the DSSC. However, the fabricated electrode showed agglomeration of PPy that seriously hinder the photovoltaic performance of the DSSC<sup>22</sup>. In this work, we have attempted to fabricate the highly dispersed PPy nanoparticles incorporated rGO counter electrode for DSSCs. To the best of our knowledge, this is the first kind of report that deals about the preparation of highly dispersed PPy nanoparticles incorporated rGO film and its application as a counter electrode for DSSC. The solar to electrical energy conversion efficiency of the rGO@PPy nanocomposite modified counter electrode based DSSC is 2.21% under AM 1.5G simulated solar irradiation of 100 mW cm<sup>-2</sup>. Further, the change in the deposition time towards the fabrication of rGO@PPy nanocomposite film, significantly accelerates the overall energy conversion efficiency of the DSSC. The remarkable electrocatalytic performance of this novel rGO@PPy nanocomposite paves the way to prepare cost-effective and highly efficient counter electrodes for Pt-free DSSCs.

## Results and discussion

**Formation of rGO@PPy nanocomposite on ITO substrate.** The electrochemical deposition of rGO@PPy on the ITO electrode was carried out by the following fabrication method. The pyrrole monomers were electrochemically oxidized for the polymerization through the initiation step during which the radical cations were formed with the delocalized radical state over the pyrrole ring. The formation of complex was achieved *via* the electrostatic charge attraction of pyrrole radical cations and pTS anions. The coupling process of pyrrole monomers was taken place by removing two protons since the more preferred location for the radical in the pyrrole ring is  $\alpha$ -position. Further growth of polymer chain was continued upon the introduction of freshly obtained radical cations on the existing oligomeric chain. Initially, the pyrrole monomers attracted the pTS anions, owing to the lower molecular density. The introduction of negatively charged GO was also attracted by the pyrrole radical cations at a slower rate, due to the higher molecular density. Concurrently, the GO was reduced to rGO upon the release of free electrons during the formation of pyrrole radical cations. The free electrons were released from the pyrrole monomer during the electrochemical oxidation of pyrrole monomers to pyrrole radical cations, and these free electrons are responsible for the reduction of the graphene oxide. It is known from previous reports<sup>23,24</sup> that during the formation of pyrrole radical cations, the free electrons that are released and it reduce the GO to rGO. The formation of PPy nanoparticles on the rGO surface was taken place through the  $\pi$ - $\pi$  stacking and the several other interactions such as Van der Waals force and hydrogen bonding.

The FESEM images of rGO@PPy nanocomposites at the deposition times of 10, 100 and 500 sec on ITO were recorded and are

shown in Figure 1. A less distribution of 25–50 nm sized PPy nanoparticles on the surface of rGO sheets at a deposition time of 10 sec is clearly observed from the Figure 1(A and B). Whereas, a uniformly distributed 30 nm sized PPy nanoparticles on the rGO sheets surface is observed for the nanocomposite film deposited at 100 sec (Figure 1(C and D)). When increasing the deposition time to 500 sec, a large amount of PPy nanoparticles with size range between 15 and 30 nm are found to be deposited on the rGO sheets (Figure 1(E and D)). The FESEM images of rGO@PPy nanocomposites suggest that changing the deposition time accelerates the distribution of PPy nanoparticles on rGO sheets during the nanocomposite formation. The difference in the PPy nanoparticles distribution on the rGO surface at different deposition times may significantly influence the electrocatalytic reactions.

**Characterization of rGO@PPy nanocomposite.** The FT-IR spectra were recorded for GO and rGO@PPy nanocomposite and are shown in Figure 2. The GO have abundant oxygen groups such as -COOH and -OH on its edges. The characteristic FT-IR peaks observed at 1734, 1626, 1404, 1224 and 1058 cm<sup>-1</sup> due to the stretching vibration of carbonyl (C=O), aromatic (C=C), carboxy (C-O), C-OH and epoxy C-O stretching vibrations, respectively of the GO sample (Figure 2(a))<sup>22</sup>. A broad and intense peak observed at 3355 cm<sup>-1</sup> is corresponding to -OH peak of GO<sup>25</sup>. The FT-IR spectrum of the rGO@PPy nanocomposite reveals that after the reduction of GO into rGO during the fabrication of rGO@PPy nanocomposite film, the peaks for the oxygen functional groups were significantly reduced/completely vanished for rGO sheets. The existing peaks at 1574 and 1224 cm<sup>-1</sup> may due to the contribution from the aromatic C=C and residual -OH<sup>26</sup>. The weak peaks were observed for rGO at 1710 and 1385 cm<sup>-1</sup>, because of the red shifted carbonyl (C=O) and carboxy (C-O) stretching vibrations feature obtained from the  $\pi$ - $\pi$  interaction between rGO sheets and PPy nanoparticles. Moreover, the peaks observed at 1514, 1430, 1119 and 1003 cm<sup>-1</sup> are corresponding to N-H bending, aromatic ring stretching, C-N stretching and N-H out-of-plane bending of PPy, reveals that successful incorporation of PPy nanoparticles on the surface of rGO in the rGO@PPy nanocomposite film (Figure 2(b))<sup>25,27</sup>.

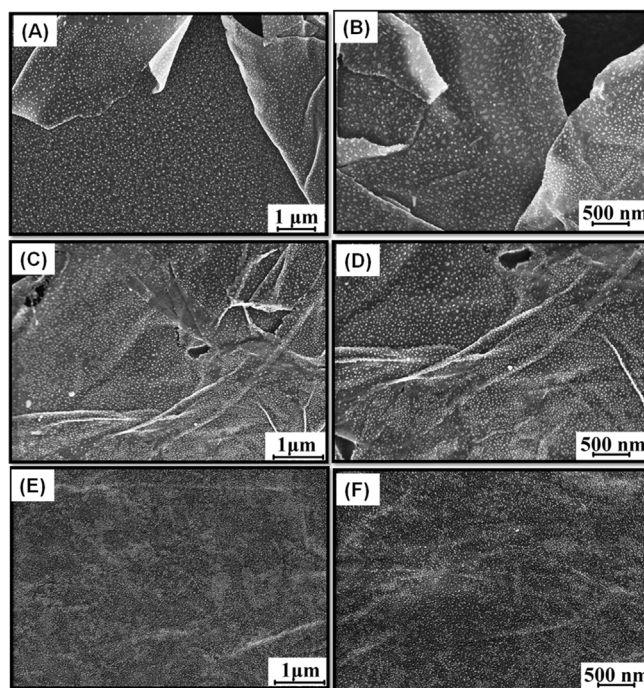


**Figure 1** | FESEM images of rGO@PPy nanocomposite films at different deposition times of (A and B) 10, (C and D) 100 and (E and F) 500 sec.

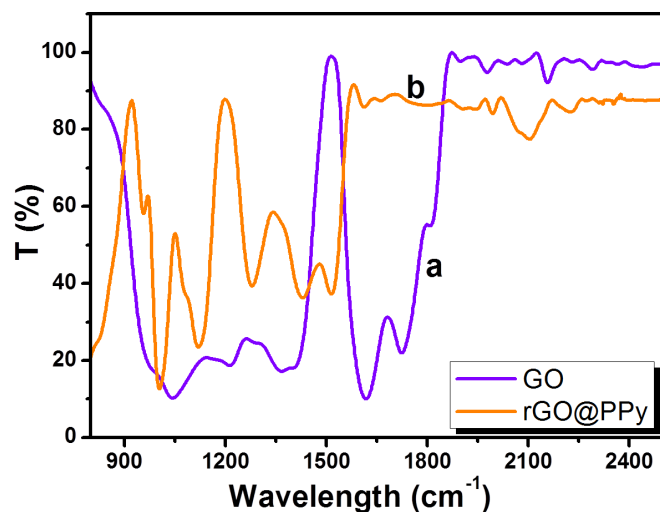


Figure 2 | FT-IR spectra of (a) GO and (b) rGO@PPy nanocomposite.

X-ray photoelectron spectroscopy (XPS) was used to confirm the functional groups present in the rGO@PPy nanocomposite film. Figure 3 shows the wide scan and de-convoluted  $C_{1s}$  core-level spectrum for GO and rGO@PPy nanocomposite. In Figure 3a, the observed peak at 399.6 eV in the entire range of XPS spectrum for rGO@PPy nanocomposite indicates the existence of nitrogen species from the PPy distributed on the surface of rGO sheets<sup>28</sup>. Meanwhile, the  $C_{1s}$  core-level spectrum of the GO could be fitted into five component peaks with binding energies of 284.3, 285.3, 286.6, 287.0 and 288.6 eV, due to the  $sp^2$  hybridized carbon,  $sp^3$  hybridized carbon, C-O, C=O and COOH species, respectively (Figure 3(b))<sup>29</sup>. Moreover, the  $C_{1s}$  core-level spectrum of the rGO@PPy nanocomposite film could be fitted into six component peaks with binding energies of 283.8, 284.5, 285, 286.2, 287.7 and 289.0 eV, due to the contribution of  $sp^2$  hybridized carbon,  $sp^3$  hybridized carbon, C-N, C-O, C=O and COOH, respectively. The oxygenated carbons were also detected in the XPS spectrum of rGO@PPy, however the intensities of these peaks are extremely reduced from those of GO, which indicates the deoxygenation of GO during the deposition process. The wide-scan XPS results revealed the absence of iron-related compounds in the nanocomposite and the absence of the XPS peak binding energy at  $\sim 700$  eV for  $FeCl_3$  and its oxides.

The Raman spectra were recorded for the GO, PPy and rGO@PPy nanocomposite and their results are shown in Figure 4. Two typical peaks in the Raman spectra were observed for the GO and rGO@PPy samples. The peak around  $1357\text{ cm}^{-1}$  (D-band) is related to the defects and disorder in the hexagonal lattice, while the  $1595\text{ cm}^{-1}$

(G-band) is due to the vibration of  $sp^2$ -bonded carbon atoms in the 2D hexagonal lattice<sup>30</sup>. Therefore, the D/G intensity ratios ( $I_D/I_G$ ) express the atomic ratio of  $sp^2/sp^3$  carbons in measuring the extent of disordered graphite. The calculated  $I_D/I_G$  ratio for GO is 0.99. For the pure PPy, the characteristic bands observed at  $1380\text{ cm}^{-1}$  and  $1577\text{ cm}^{-1}$  due to the ring stretching mode and the C=C backbone stretching of PPy, respectively<sup>31</sup>. In addition, the peak at  $928\text{ cm}^{-1}$  and two small peaks at  $964\text{ cm}^{-1}$  and  $1060\text{ cm}^{-1}$  are due to the bipolaron ring deformation and the polaron symmetric C-H in-plane bending vibration, respectively<sup>32,33</sup>. The calculated  $I_D/I_G$  ratio is 0.88. The Raman spectrum of the rGO@PPy nanocomposite showed the bands for PPy, and proven that the presence of PPy nanoparticles in the nanocomposite. Furthermore, the decrease of the  $I_D/I_G$  value (0.82) of nanocomposite showed that the disordered of graphene is lesser and with the support of peak shift of G-band from  $1590\text{ cm}^{-1}$  to  $1570\text{ cm}^{-1}$  compared to GO confirm the reduction of GO during electrodeposition process<sup>34</sup>.

**Photovoltaic performance of rGO@PPy counter electrode based DSSCs.** The photovoltaic performances of the rGO@PPy based counter electrode based DSSCs (Figure 5A) were investigated under a simulated solar irradiation of  $100\text{ mW/cm}^2$  (AM 1.5G). The photocurrent density-photovoltage (J-V) profile is used to examine critical photovoltaic parameters such as open-circuit voltage ( $V_{oc}$ ), short-circuit photocurrent density ( $J_{sc}$ ), maximum photovoltage ( $V_{max}$ ) and maximum photocurrent density ( $J_{max}$ ). The fill factor (FF) and power conversion efficiency ( $\eta$ ) of the DSSC can be obtained from the Eqns. 1 and 2, respectively<sup>35</sup>.

$$FF = \frac{V_m J_m}{V_{oc} J_{sc}} \quad (1)$$

$$\eta = \frac{V_{oc} J_{sc} FF}{I_s} \quad (2)$$

where,  $I_s$  is the intensity of the incident light.

To evaluate the photovoltaic performance of the DSSC, the photocurrent density-photovoltage (J-V) curves were recorded for the rGO@PPy based counter electrode and are shown in Figure 5B and their corresponding photovoltaic parameters are listed in Table 1. The obtained conversion efficiencies DSSCs with rGO@PPy nanocomposite counter electrode prepared at different deposition times of 10, 50, 100, 250 and 500 sec are 0.85, 1.06, 2.21, 1.15 and 0.39%, respectively. In order to obtain an efficient DSSC, optimizing the deposition time of rGO@PPy counter electrode is essential. In this respect, the deposition time for rGO@PPy was varied to obtain the counter electrode with optimum performance in DSSC. The observed results clearly revealed that the conversion efficiency of DSSCs was increased while increasing the deposition time until it

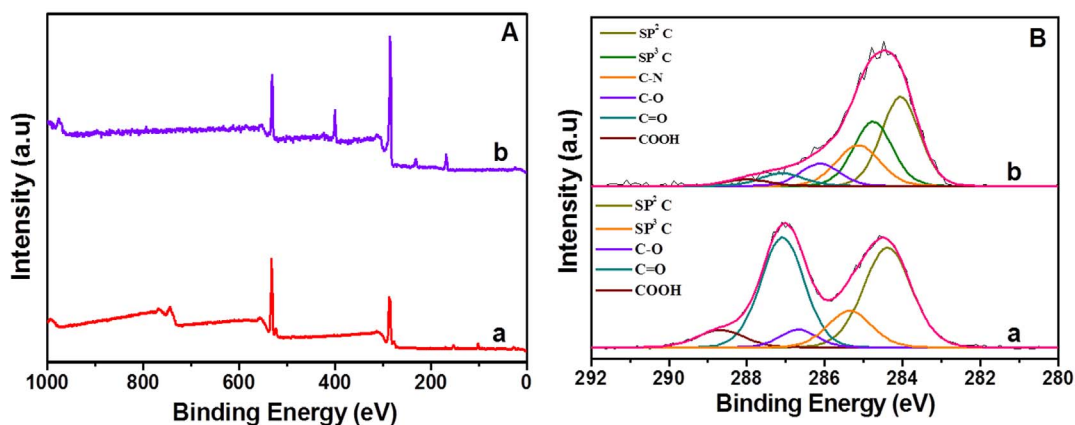
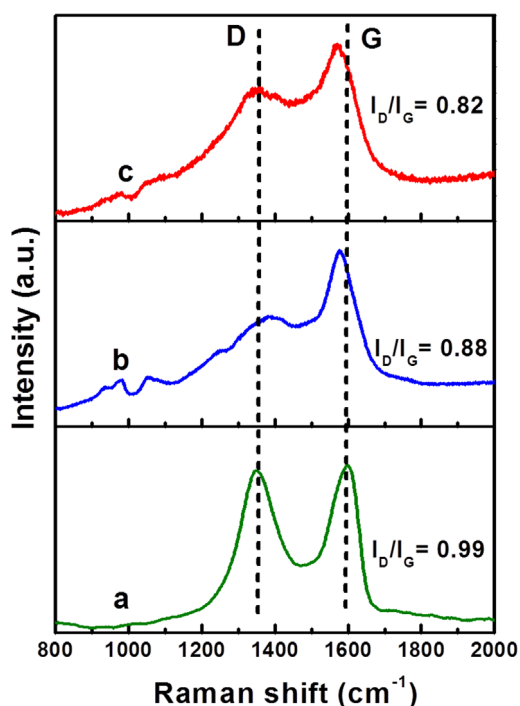


Figure 3 | (A) Wide scan XPS and (B)  $C_{1s}$  core-level spectra of the (a) GO and (b) rGO@PPy nanocomposite.



**Figure 4** | Raman spectra obtained for the (a) GO, (b) PPy and (c) rGO@PPy nanocomposite.

reached a maximum of 100 sec. The increase in the efficiency is due to the increase in the number of PPy nanoparticles on the rGO sheets, which consequently improved the  $J_{sc}$  of the device. This phenomenon can be attributed to the fact that the electrocatalytic activity of rGO@PPy continually increases with increasing the PPy content in the nanocomposite. Further increase in the deposition time led to decrease in the conversion efficiency (Figure 6a). The decrease in the efficiency for higher deposition time can be ascribed to the distribution of large number of PPy nanoparticles on the rGO sheets that leads to decrease in catalytic activity towards the reduction of  $I_3^-$  into  $I^-$  ions and to regenerate the oxidized dye after the electron injection process. As a consequence, the overall energy conversion efficiency of DSSC was deteriorated. The  $J_{sc}$  was increased while increasing the deposition time and attained a maximum of 2.21 mA/cm<sup>2</sup> at the

**Table 1** | Photovoltaic parameters of the rGO@PPy counter electrode based DSSCs

Deposition time (s)	$J_{sc}$ (mA/cm <sup>2</sup> )	$V_{oc}$ (V)	$J_{max}$ (mA/cm <sup>2</sup> )	$V_{max}$ (V)	FF	$\eta$ (%)
10	2.49	0.68	1.83	0.47	0.51	0.85
50	4.82	0.68	3.03	0.35	0.32	1.06
100	7.49	0.70	5.40	0.41	0.42	2.21
250	3.78	0.66	2.34	0.49	0.46	1.15
500	2.49	0.44	1.54	0.25	0.36	0.39

**Foot note:** The DSSCs performance was evaluated under 100 mW cm<sup>-2</sup> simulated AM 1.5G solar light irradiation.  $J_{sc}$ : Short-circuit photocurrent density;  $V_{oc}$ : Open-circuit photovoltage;  $J_{max}$ : Maximum photocurrent density;  $V_{max}$ : Maximum photovoltage; FF: Fill factor;  $\eta$ : Power conversion efficiency. Area of the cell was 0.5 cm<sup>2</sup>.

deposition time of 100 sec (Figure 6b). Further increase in the deposition time to 250 sec decreased the  $J_{sc}$  value to ~0.39 mA/cm<sup>2</sup>. It can also be seen that the  $V_{oc}$  trends were frustrate within the range of ~0.44 and 0.70 V. The  $J_{max}$  and  $V_{max}$  values of the device were also followed the similar trends exhibited by the  $J_{sc}$  and  $V_{oc}$  (Figure 6c).

In order to understand the suitability of best rGO@PPy nanocomposite based counter electrode with deposition time of 100 sec, the J-V curve for the sputtered Pt based DSSC was recorded and are shown in Figure 7. When compared to DSSC with Pt counter electrode, the photovoltaic parameters of the rGO@PPy based DSSC were increased (Table 2). The overall solar to electrical energy conversion efficiency of the DSSC with rGO@PPy counter electrode was 2.21%, which was higher than that of the DSSC with sputtered Pt counter electrode (2.19%). The improved photovoltaic performances exhibited by the DSSC with rGO@PPy based counter electrode is due to the highly dispersed PPy nanoparticles on the rGO surface that facilitate high electrocatalytic activity for the  $I_3^-/I^-$  redox reaction.

Khamson *et al.* reported that a DSSC with a polypyrrole film was used as a counter electrode and showed a conversion efficiency of 4.72% which is lower than a platinum counter electrode (7.59%)<sup>36</sup>. Zhang *et al.* reported a graphene based counter electrode with an efficiency of 6.81%. However, this was still lower than the platinum sample (7.59%)<sup>37</sup>. Few works have reported the use of graphene-incorporated polypyrrole as a counter electrode and it's shown that a conversion efficiency of ~8% has been achieved. However, the obtained efficiency is still lower than that of the Pt-based counter

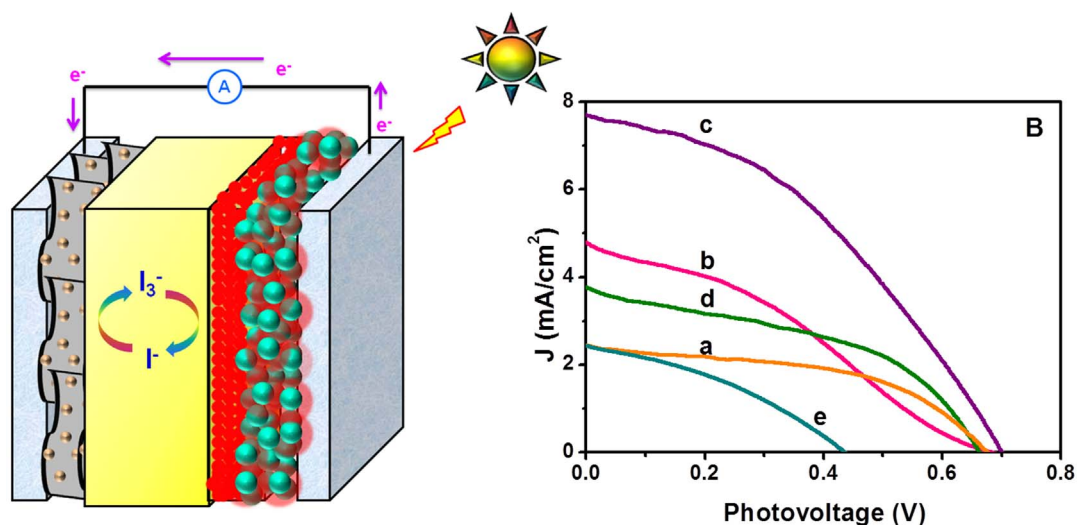


**Figure 5** | (A) Configuration of rGO@PPy counter electrode based DSSC and (B) Photocurrent density-photovoltage (J-V) curves obtained under simulated solar irradiation of AM 1.5 G (100 mW/cm<sup>2</sup>) for the DSSCs having the TiO<sub>2</sub>/N719/Iodolyte configuration integrated with rGO@PPy nanocomposite based counter electrodes prepared at deposition times of (a) 10, (b) 50, (c) 100, (d) 250 and (e) 500 sec.

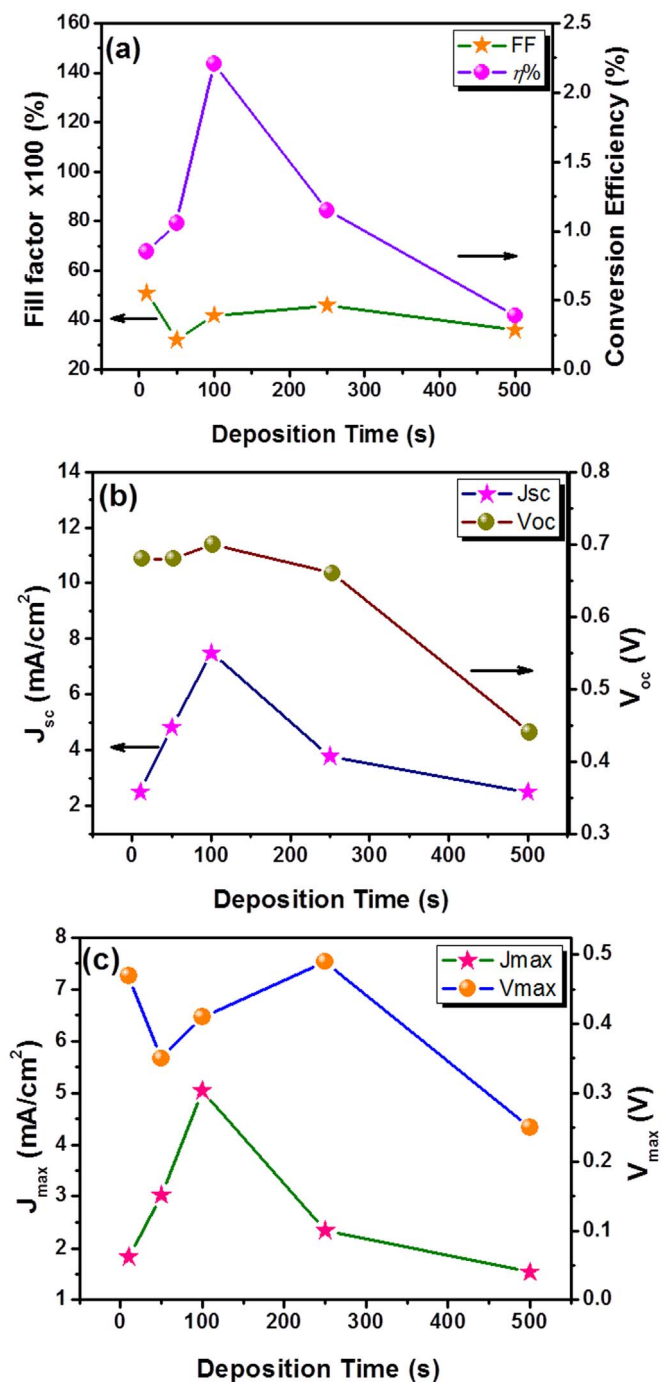


**Figure 6** | Plots of (A) Fill factor (FF) and power conversion efficiency ( $\eta$ ), (B) short-circuit photocurrent density ( $J_{sc}$ ) and open-circuit photovoltage ( $V_{oc}$ ) and (C) maximum photocurrent density ( $J_{max}$ ) and maximum photovoltage ( $V_{max}$ ) with different rGO content.

electrode. Chen *et al.* reported a graphene-based counter electrode with an efficiency of 5.27%. However, this was lower than that of the platinum (6.02%)<sup>17</sup>. Gong *et al.* reported that a DSSC with a polypyrrole film was used as a counter electrode, and it showed a lower conversion efficiency (8.14%) than a platinum counter electrode (8.34%)<sup>22</sup>. Even though the reported DSSCs were shown high efficiency but still it is lower when compared to the Pt based DSSC<sup>17,22,36,37</sup>. In this work, the rGO@PPy counter electrode showed the efficiency of 2.21%, which was higher than that of the DSSC with sputtered Pt counter electrode (2.19%).

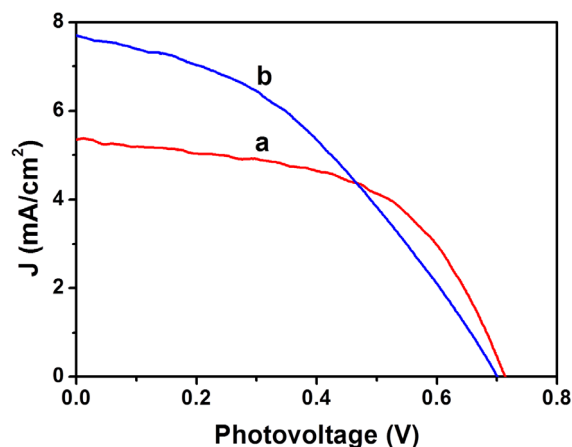


**Figure 7** | Photocurrent density-photovoltage (J-V) curves obtained under simulated solar irradiation of AM 1.5 G (100 mW/cm<sup>2</sup>) for the DSSCs having the TiO<sub>2</sub>/N719/Iodolyte configuration integrated with (a) sputtered Pt and (b) PPyr@rGO based counter electrode.

**Electrochemical characterizations.** Electrochemical impedance spectroscopic (EIS) measurements were performed to investigate the electrochemical behavior of the rGO@PPy counter electrode. Figure 8 shows Nyquist plots obtained for the rGO@PPy counter electrodes prepared at different deposition times. The Nyquist plots showed semicircles, which are due to the charge-transfer resistance ( $R_{ct}$ ) that takes place at the rGO@PPy/electrolyte interface. The charge-transfer resistance induces negative impact on the photovoltaic parameters such as FF and overall efficiency. The photovoltaic performances of DSSCs crucially depend on the  $R_{ct}$  values which were fabricated with same anodes, dye and electrolyte but rGO@PPy counter electrode with different deposition times. It can be obviously seen that the  $R_{ct}$  was decreased while increasing the deposition time from 10 to 500 sec and this can be attributed to the corresponding increase in the PPy nanoparticles on the surface of rGO sheets. When the deposition time was 10 sec, less number of PPy nanoparticles was distributed on the rGO sheets that led to the poor electrical conductivity between redox couple and counter electrode, resulted in larger  $R_{ct}$  value and lower photovoltaic performance.

As shown in the Bode phase plots, the frequency angle of the mid-frequency peak ( $f_{mid}$ ) decreases with an increase in the deposition time during the fabrication of rGO@PPy nanocomposites, which indicated that the electron life time, is elongated in the deposition time range from 50 to 500 sec (Figure 8(B)). However, the rGO@PPy nanocomposite prepared at a deposition time of 100 sec shows a short frequency angle when compared to the rGO@PPy nanocomposite prepared at 500 sec. We believed that a very large number of PPy nanoparticles distributed on the rGO sheets may be responsible for this behavior. The increase in the deposition time induces large charge-transfer resistance to some perturbation for electrolyte diffusion, which greatly influences the impedance behavior in this region. The EIS was recorded for the sputtered Pt electrode and its Nyquist plot along with the rGO@PPy nanocomposite modified electrode is shown in Figure 8(C). Interestingly, the  $R_{ct}$  value of rGO@PPy electrode was found to be 14.8  $\Omega$  cm<sup>2</sup>, which was comparable to that of the sputtered Pt electrode (14.3  $\Omega$  cm<sup>2</sup>), indicating that the identical intrinsic catalytic activities take place on the surface of rGO@PPy electrode for the reduction of I<sub>3</sub><sup>-</sup>. The similar  $R_{ct}$  value obtained for rGO@PPy electrode to that of the sputtered Pt electrode suggests that it could be a competitive counter electrode material to the high-cost platinum.

## Conclusions

The PPy nanoparticles incorporated rGO based counter electrodes were fabricated via an in-situ electrochemical deposition method for

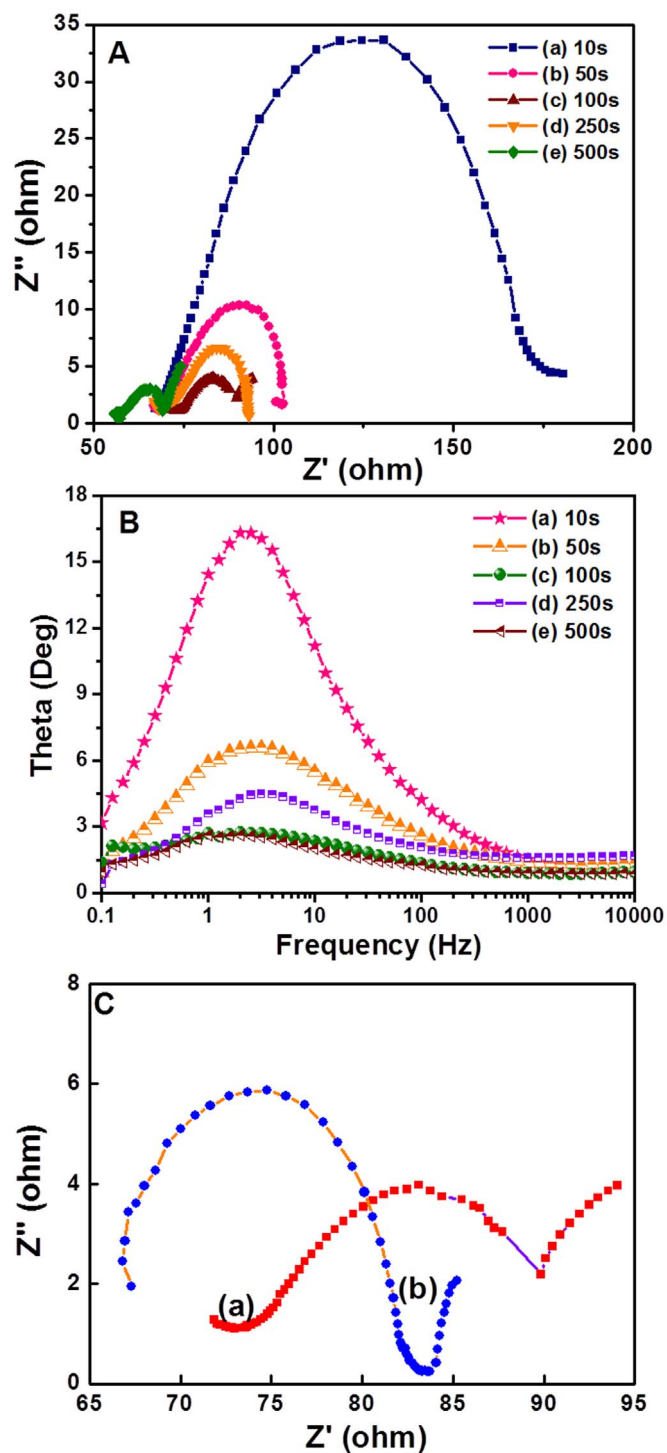


**Figure 8** | (A) Nyquist plots and (B) Bode phase plots obtained for the rGO@PPy nanocomposite based counter electrodes prepared at deposition times of (a) 10, (b) 50, (c) 100, (d) 250 and (e) 500 sec. (C) Nyquist plots obtained for the (a) sputtered Pt and (b) rGO@PPy nanocomposite at deposition time of 100 sec.

the Pt-free DSSC. The SEM images showed uniform distribution of PPy nanoparticles with diameter in the range of 20–30 nm on the rGO sheets. When increasing the deposition time, large number of PPy nanoparticles was found to be deposited on the rGO surface. The electrochemical studies revealed that the rGO@PPy had smaller charge-transfer resistance and similar electrocatalytic activity for the  $I_3^-/I^-$  redox reaction in DSSC. The overall solar to electrical energy conversion efficiency of the DSSC based on the rGO@PPy

**Table 2** | Photovoltaic parameters of the fabricated DSSCs

Counter Electrode	$J_{sc}$ ( $mA/cm^2$ )	$V_{oc}$ (V)	$J_{max}$ ( $mA/cm^2$ )	$V_{max}$ (V)	FF	$\eta$ (%)
Sputtered Pt	5.12	0.71	4.31	0.51	0.60	2.19
rGO@PPy	7.49	0.70	5.40	0.41	0.42	2.21

**Foot note:** The DSSCs performance was evaluated under  $100\text{ mW cm}^{-2}$  simulated AM 1.5G solar light irradiation.  $J_{sc}$ : Short-circuit photocurrent density;  $V_{oc}$ : Open-circuit photovoltage;  $J_{max}$ : Maximum photocurrent density;  $V_{max}$ : Maximum photovoltage; FF: Fill factor;  $\eta$ : Power conversion efficiency. Area of the cell was  $0.5\text{ cm}^2$ .

counter electrode was 2.21%, which was merely equal to that of the DSSC with Pt counter electrode (2.19%). The optimized deposition time for rGO@PPy to obtain higher conversion efficiency in DSSC was 100 sec. The low-cost, excellent performance, rapid and simple fabrication methods of the rGO@PPy modified counter electrode proved to be a potential alternative to the high-cost Pt as counter electrode in DSSC.

## Methods

**Materials.** Titanium dioxide (P25) and pyrrole were purchased from Acros Organics. Graphite flakes were obtained from Ashbury Inc., USA. Common chemicals, such as toluene-4-sulfonic acid sodium salt (NapTS), sulphuric acid ( $H_2SO_4$ , 98%), phosphoric acid ( $H_3PO_4$ , 85%), potassium permanganate ( $KMnO_4$ , 99.9%), iron (III) chloride ( $FeCl_3$ ) and hydrogen peroxide ( $H_2O_2$ , 30%) were procured from Merck and used as such. Indium doped tin oxide (ITO) coated conducting glass slides ( $7\ \Omega/sq$ ) were supplied by Xin Yan Technology Limited, China. N719 (Ruthenizer 535-bisTBA) and Iodolyte Z-100 were received from Solaronix.

**Materials characterization techniques.** X-ray photoelectron spectroscopy (XPS) measurement was carried out using Axis Ultra<sup>DL</sup> (Kratos analytical Ltd). The surface morphology of the rGO@PPy nanocomposite films were examined by using Hitachi SU 8000 field emission scanning electron microscopy. The FT-IR spectral data were obtained from Perkin-Elmer-1725x FT-IR spectrophotometer. The Raman spectra were recorded using a Renishaw 2000 (inVia) system with an argon ion laser emitting at 532 nm. The electrochemical and photocurrent measurements were performed in a computer-controlled Versa STAT 3 electrochemical workstation (Princeton Applied Research, USA).

**Fabrication of rGO@PPy counter electrode.** The rGO@PPy nanocomposite films were fabricated by a catalyst-assisted in-situ electrochemical polymerization method. Briefly, pyrrole (0.1 M), GO (1 mg/mL), NapTS (0.1 M) and  $FeCl_3$  (0.1 M) were mixed in an electrochemical cell and vigorously stirred for 5 min in order to obtain a PPy nanoparticles in the solution. After the formation of PPy nanoparticles, the rGO@PPy nanocomposite films were deposited at a constant applied potential of +0.8 V by using potentiostat-galvanostat (Elchema model EQCN-502 Faraday cage) at room temperature and at different deposition times (10, 50, 100, 250 and 500 sec). After electrodeposition, the films were thoroughly rinsed with high pure de-ionized water five times to remove any impurities related to the iron salts. For the electrodeposition experiments, indium doped tin oxide, graphite and saturated calomel electrode were employed as working, counter and reference electrodes, respectively.

**Fabrication of DSSCs and their performance evaluation.** The  $TiO_2$  photoanodes were fabricated by the following procedure. Initially, 300 mg of P25 was mixed with 5 mL of ethanol which was stirred for 30 min to obtain a homogenous solution. A 0.1 M of TTIP was slowly introduced into the above reaction mixture under ultrasonication. The obtained  $TiO_2$  paste was coated on the conducting side of ITO by adopting doctor-blade method. A 3M scotch tape with a thickness of 55  $\mu m$  was used for the photoanode fabrication. The  $TiO_2$  film was dried at room temperature, sintered at  $150^\circ C$  for 10 min in a muffle furnace and then allowed to cool naturally up to  $80^\circ C$ . The photoanode was immersed in the ethanolic solution of 0.3 mM N719 (Ruthenizer 535-bisTBA) dye for 24 h. The dye-adsorbed photoanode was withdrawn from the solution and immediately cleaned/rinsed with ethanol. The newly prepared rGO@PPy nanocomposite film (approximately 3  $\mu m$  thickness (Figure S1)) was placed on the dye-adsorbed photoanode and then clamped firmly together. Meltonix 1170-60PF (Solaronix) with a  $\sim 60\text{-}\mu m$ -thick spacer was used. A redox electrolyte (Iodolyte Z-100, Solaronix) solution was introduced into the cell assembly by capillary action. The DSSC with an active area of  $0.5\text{ cm}^2$  was used to measure its performance. Prior to test the photovoltaic parameters, Avaspec-2048 fibre optic spectrophotometer was used to measure the simulated light intensity.

1. Thomas, S. *et al.* A review on counter electrode materials in dye-sensitized solar cells. *J. Mater. Chem. A* **2**, 4474–4490 (2014).



2. Joshi, P. *et al.* Electrospun carbon nanofibers as low-cost counter electrode for dye-sensitized solar cells. *ACS Appl. Mater. Interfaces* **2**, 3572–3577 (2010).
3. Dong, P. *et al.* Vertically aligned single-walled carbon nanotubes as low-cost and high electrocatalytic counter electrode for dye-sensitized solar cells. *ACS Appl. Mater. Interfaces* **3**, 3157–3161 (2011).
4. Han, J. *et al.* Water-soluble polyelectrolyte-grafted multiwalled carbon nanotube thin films for efficient counter electrode of dye-sensitized solar cells. *ACS Nano* **4**, 3503–3509 (2010).
5. Balamurugan, J., Pandurangan, A., Thangamuthu, R. & Senthilkumar, S. M. Effective synthesis of well-graphitized carbon nanotubes on bimetallic SBA-15 template for use as counter electrode in dye-sensitized solar cells. *Ind. Eng. Chem. Res.* **52**, 384–393 (2012).
6. Sun, H. *et al.* In situ preparation of a flexible polyaniline/carbon composite counter electrode and its application in dye-sensitized solar cells. *J. Phys. Chem. C* **114**, 11673–11679 (2010).
7. Kang, D.-Y., Lee, Y., Cho, C.-Y. & Moon, J. H. Inverse opal carbons for counter electrode of dye-sensitized solar cells. *Langmuir* **28**, 7033–7038 (2012).
8. Veerappan, G., Bojan, K. & Rhee, S.-W. Sub-micrometer-sized graphite as a conducting and catalytic counter electrode for dye-sensitized solar cells. *J. Am. Chem. Soc.* **3**, 857–862 (2011).
9. Li, Z. *et al.* Facile electropolymerized-PANI as counter electrode for low cost dye-sensitized solar cell. *Electrochem. Commun.* **11**, 1768–1771 (2009).
10. Wu, J. *et al.* An all-solid-state dye-sensitized solar cell-based poly(N-alkyl-4-vinylpyridine iodide) electrolyte with efficiency of 5.64%. *J. Am. Chem. Soc.* **130**, 11568–11569 (2008).
11. Wu, M. *et al.* Economical Pt-free catalysts for counter electrodes of dye-sensitized solar cells. *J. Am. Chem. Soc.* **134**, 3419–3428 (2012).
12. Gong, F. *et al.* In situ growth of Co<sub>0.85</sub>Se and Ni<sub>0.85</sub>Se on conductive substrates as high-performance counter electrodes for dye-sensitized solar cells. *J. Am. Chem. Soc.* **134**, 10953–10958 (2012).
13. Imoto, K. *et al.* High-performance carbon counter electrode for dye-sensitized solar cells. *Sol. Energy Mater. Sol. Cells* **79**, 459–469 (2003).
14. Murakami, T. N. & Grätzel, M. Counter electrodes for DSC: Application of functional materials as catalysts. *Inorg. Chim. Acta* **361**, 572–580 (2008).
15. Banks, C. E., Davies, T. J., Wildgoose, G. G. & Compton, R. G. Electrocatalysis at graphite and carbon nanotube modified electrodes: edge-plane sites and tube ends are the reactive sites. *Chem. Commun.* 829–841 (2005).
16. Xu, Y. *et al.* Flexible graphene films via the filtration of water-soluble noncovalent functionalized graphene sheets. *J. Am. Chem. Soc.* **130**, 5856–5857 (2008).
17. Chen, L. *et al.* Graphene quantum-dot-doped polypyrrole counter electrode for high-performance dye-sensitized solar cells. *ACS Appl. Mater. Interfaces* **5**, 2047–2052 (2013).
18. Wang, G., Zhuo, S. & Xing, W. Graphene/polyaniline nanocomposite as counter electrode of dye-sensitized solar cells. *Mater. Lett.* **69**, 27–29 (2012).
19. Lee, K. S. *et al.* Flexible and platinum-free dye-sensitized solar cells with conducting-polymer-coated graphene counter electrodes. *ChemSusChem* **5**, 379–382 (2012).
20. Hong, W. *et al.* Transparent graphene/PEDOT–PSS composite films as counter electrodes of dye-sensitized solar cells. *Electrochem. Commun.* **10**, 1555–1558 (2008).
21. Wu, J. *et al.* High-performance polypyrrole nanoparticles counter electrode for dye-sensitized solar cells. *J. Power Sources* **181**, 172–176 (2008).
22. Gong, F., Xu, X., Zhou, G. & Wang, Z.-S. Enhanced charge transportation in a polypyrrole counter electrode via incorporation of reduced graphene oxide sheets for dye-sensitized solar cells. *Phys. Chem. Chem. Phys.* **15**, 546–552 (2013).
23. Lim, Y. S. *et al.* Preparation and characterization of polypyrrole/graphene nanocomposite films and their electrochemical performance. *J. Polym. Res.* **20**, 1–10 (2013).
24. Lim, Y. S. *et al.* Potentiostatically deposited polypyrrole/graphene decorated nano-manganese oxide ternary film for supercapacitors. *Ceram. Int.* **40**, 3855–3864 (2014).
25. Han, Y., Hao, L. & Zhang, X. Preparation and electrochemical performances of graphite oxide/polypyrrole composites. *Synth. Met.* **160**, 2336–2340 (2010).
26. Bose, S. *et al.* In-situ synthesis and characterization of electrically conductive polypyrrole/graphene nanocomposites. *Polym.* **51**, 5921–5928 (2010).
27. Jamadade, S., Jadhav, S. V. & Puri, V. Electromagnetic reflection, shielding and conductivity of polypyrrole thin film electropolymerized in P-Tulensulfonic acid. *J. Non-Cryst. Solids* **357**, 1177–1181 (2011).
28. Amarnath, C. A. *et al.* Efficient synthesis of graphene sheets using pyrrole as a reducing agent. *Carbon* **49**, 3497–3502 (2011).
29. Yumitori, S. Correlation of C1s chemical state intensities with the O1s intensity in the XPS analysis of anodically oxidized glass-like carbon samples. *J. Mater. Sci.* **35**, 139–146 (2000).
30. Lim, S. P., Huang, N. M. & Lim, H. N. Solvothermal synthesis of SnO<sub>2</sub>/graphene nanocomposites for supercapacitor application. *Ceram. Int.* **39**, 6647–6655 (2013).
31. Sahoo, N. G., Jung, Y. C., So, H. H. & Cho, J. W. Polypyrrole coated carbon nanotubes: Synthesis, characterization, and enhanced electrical properties. *Synth. Met.* **157**, 374–379 (2007).
32. Duchet, J., Legras, R. & Demoustier-Champagne, S. Chemical synthesis of polypyrrole: structure-properties relationship. *Synth. Met.* **98**, 113–122 (1998).
33. Furukawa, Y., Tazawa, S., Fujii, Y. & Harada, I. Raman spectra of polypyrrole and its 2,5-13C-substituted and C-deuterated analogues in doped and undoped states. *Synth. Met.* **24**, 329–341 (1988).
34. Chen, W., Yan, L. & Bangal, P. R. Chemical reduction of graphene oxide to graphene by sulfur-containing compounds. *J. Phys. Chem. C* **114**, 19885–19890 (2010).
35. Lim, S. P., Huang, N. M., Lim, H. N. & Mazhar, M. Surface modification of aerosol-assisted CVD produced TiO<sub>2</sub> thin film for dye sensitised solar cell. *Int. J. Photoenergy* **2014**, 12 (2014).
36. Keothongkham, K. *et al.* Electrochemically deposited polypyrrole for dye-sensitized solar cell counter electrodes. *Int. J. Photoenergy* **2012** (2012).
37. Zhang, D. W. *et al.* Graphene-based counter electrode for dye-sensitized solar cells. *Carbon* **49**, 5382–5388 (2011).

## Acknowledgments

This work was financially supported by ERGS grant (ER008-2012A); the Science Fund from the Ministry of Science, Technology and Innovation (06-01-04-SF1513); and a High Impact Research Grant from the Ministry of Higher Education of Malaysia (UM.C/625/1/HIR/MOHE/SC/21).

## Author contributions

S.P.L., Y.S.L. and A.P. designed the experiment and project. S.P.L. prepared the photoanode and Y.S.L. prepared the counter electrodes. A.P. and S.P.L. wrote the main manuscript text. S.P.L. and Y.S.L. prepared all the figures. S.P.L. analysed and wrote the manuscript part regarding the photovoltaic performance of the device, Y.S.L. and A.P. analysed and wrote the characterization part of the counter electrodes. N.M.H. and H.N.L. reviewed the manuscript content. All authors participated in the discussion and commented on the paper.

## Additional information

**Supplementary information** accompanies this paper at <http://www.nature.com/scientificreports>

**Competing financial interests:** The authors declare no competing financial interests.

**How to cite this article:** Lim, S.P., Pandikumar, A., Lim, Y.S., Huang, N.M. & Lim, H.N. In-situ electrochemically deposited polypyrrole nanoparticles incorporated reduced graphene oxide as an efficient counter electrode for platinum-free dye-sensitized solar cells. *Sci. Rep.* **4**, 5305; DOI:10.1038/srep05305 (2014).



This work is licensed under a Creative Commons Attribution-NonCommercial-ShareAlike 4.0 International License. The images or other third party material in this article are included in the article's Creative Commons license, unless indicated otherwise in the credit line; if the material is not included under the Creative Commons license, users will need to obtain permission from the license holder in order to reproduce the material. To view a copy of this license, visit <http://creativecommons.org/licenses/by-nc-sa/4.0/>